Early Earth zircons formed in residual granitic melts produced by the upper crustal crystallization of tonalite

Oscar LAURENT*, Jean-François MOYEN, Jörn-Frederik WOTZLAW, Jana BJÖRNSEN, Olivier BACHMANN
*corresponding author: oscar.laurent@get.omp.eu

This supplemental material file includes:

1. Analytical methods
2. Details about analyzed samples and compiled data
3. Proxies used to filter zircon trace element data for the effects of alteration
4. Details about the zircon/melt partitioning model
5. Methods for thermodynamic modelling of tonalite crystallization

Other Supplementary Data: Supplementary Data file DR2 [zircon trace element data from the Barberton plutonic-volcanic suite and compilation of Hadean-Archean zircon compositions]

1. Analytical methods

Zircons were extracted from crushed samples using conventional separation techniques, mounted in Epoxy mounts and polished. Analysis of trace elements was carried out by LA-ICP-MS at ETH Zürich, Switerzland, using a RESOlution excimer 193 nm (ArF) laser ablation system (ASI/Applied Spectra) attached to an Element XR (Thermo Scientific) sector-field ICP-MS. We used a laser spot diameter of 19 µm, energy density of ca. 2 $J \cdot cm^{-2}$ and repetition rate of 5 Hz. The sample surface was cleaned before each analysis by three pre-ablation pulses. Ablation was performed in a dual-volume, fast-washout S-155 ablation cell (Laurin Technic) fluxed with carrier gas consisting of high-purity He (ca. 0.5 $L \cdot min^{-1}$), mixed in the ablation funnel with make-up gas consisting of high-purity Ar (ca. 1 $L \cdot min^{-1}$). The ablated aerosol was homogenized via flushing through an in-house made squid device before being introduced in the plasma.

A total of 105 mass scans (ca. 0.59 s each) were acquired over ca. 60 s measurement (20 s gas blank followed by 40 s ablation). Trace element data and U-Pb dates were acquired simultaneously from the same spots; the results of U-Pb dating are already reported and discussed in Laurent et al. (2020). For trace element quantification, we collected intensities at amu 7, 27, 29, 31, 43, 49, 89, 91, 93, 138, 139, 140, 141, 146, 147, 153, 157, 159, 163, 165, 166, 169, 172, 175, 178, 181, 204, 232 and 238 (intensities at amu 202, 206, 207 and 208 were used for dating only) with dwell times of 10 ms, except at amu 27, 29, 31, 43, 89, 91, 93, 138, 181 (5 ms) and 49 (25 ms).

The glass reference material NIST SRM610 (Jochum et al., 2011) was used as primary reference material for trace element quantification and for the correction of instrumental drift, using conventional standard-sample bracketing. We used the stoechiometric Si content of zircon (15.2 wt.%) as internal standard for relative sensitivity correction. The data were processed with the Igor Pro-based Iolite software v2.5 (Hellstrom et al., 2008) using the built-in data reduction scheme for trace elements and using the same integration intervals (for unknowns and reference materials) as previously defined for U-Pb dating. This procedure warrants that trace element concentrations and U-Pb dates are obtained from exactly the same sample volume.

The accuracy and reproducibility of the analyses were checked by repeated measurements of zircon reference materials 91500 (Widenbeck et al., 1995), AUSZ7-1 (Kennedy et al., 2014) and Plešovice (Slamá et al., 2008). A further matrix correction factor was specifically applied for Ti to ensure the accuracy of the results for purposes of thermometry, by normalizing the Ti content of 91500 determined by ID-ICP-MS (4.73 ppm; Szymanowski et al., 2017) to the raw, average Ti content measured here (4.16 ± 0.75 ppm, 2 S.D., n = 15).

The full dataset is provided in the Supplementary Data file DR2. Representative cathodoluminescence images of zircons and a full report of U-Pb isotopic data can be found in Laurent et al. (2020).

2. Details about analyzed samples and compiled data

Table S1: Location, nature, mineralogy and age (from Laurent et al., 2020) of samples of the Paleoarchean Barberton volcanic-plutonic suite used here to investigate zircon trace element compositions.

Sample	Latitude S	Longitude E	Geological Unit	Rock type	U-Pb zircon age (Ma) [a]	Mineralogy [b]
JB17-C2a	26°01.50'	30°49.64'	Theespruit	Trondhjemite	3460 ± 8	Pl, Qz, Kfs, Bt/Chl, Amp (Ap, Ep, Ttn, OP, Zrn)
JB17-C2d	26°01.45'	30°49.67'	Theespruit	Diorite	3460 ± 6	Pl, Amp, Qz, Bt/Chl, Kfs (Ttn, Ap, OP, Zrn)
JB17-C5b	26°01.49'	30°45.71'	Stolzburg	Tonalite	3454 ± 15	Pl, Amp, Qz, Bt/Chl, Kfs (Ttn, OP, Ap, Zrn)
JB17-C6	26°00.50'	30°43.99'	Stolzburg	Trondhjemite	3456 ± 10	Pl, Qz, Kfs, Bt/Chl (Ep, Ap, Zrn)
JB17-D1a	26°05.40'	30°44.00'	Gneissic zone	Trondhjemite	3434 ± 18	Pl, Qz, Kfs, Bt/Chl (Amp, Ep, Ap, Zrn)
JB17-D2a	26°01.15'	30°51.58'	Doornhoek	Granite	3426 ± 19	Pl, Qz, Kfs, Bt/Chl (Ep, Ap, Zrn)
JB17-D3a	26°01.46'	30°50.83'	Theespruit	Granite (dyke)	3470 ± 18	Pl, Qz, Kfs (Bt/Chl, Ep, Ap, Zrn)
JB17-F2	25°56.40'	30°53.62'	BRVC [c]	Rhyolite (altered)	3455 ± 11	Pl*, Qz, Gm* (OP*, Ap, Zrn)
JB17-F5	25°56.11'	30°53.71'	BRVC [c]	Rhyolite (altered)	3429 ± 25	Pl*, Qz, Bt*/Chl* (OP*, Gm*, Ap, Zrn)

[a]U-Pb crystallization age from Laurent et al. (2020); [b]Minerals listed by order of decreasing abundance; minor and accessory phases in brackets (abbreviations after Whitney and Evans, 2010); [c]BRVC = Buck Ridge Volcanic Complex; *Phase partly or totally transformed to secondary alteration products in the volcanic rocks.

Table S2: Sources of data for the zircon trace element compilation and details about the corresponding samples.

Reference	Igneous rock type	Craton, country	Geological Unit	Age (Ga)[a]	Ns [b]	Nz [c]	WR data[d]
Igneous (TTG-hosted) zircon							
This study	Diorite, tonalite trondhjemite, granite, rhyolite	Kalahari (Kaapvaal), South Africa	Barberton Granitoid-Greenstone Terrain	3.46	9	372	Yes
Bouvier et al. (2012)	Qz-diorite, tonalite	Superior Province, Canada	English River, Wawa and Wabigoon subprovinces	2.73-2.69	4	21	Partly
Kielman et al. (2018)	Tonalite	North Atlantic, Greenland	Nuuk region, Itsaq Gneiss Complex	3.85	1	48	Yes
Kitajima et al. (2012)	Rhyolite	Pilbara, Australia	North Pole Dome	3.45	1	34	Yes
Liu et al. (2013) [e]	Tonalite, granite gneiss	North China	Jiaobei Province	2.55	6 [e]	148 [e]	No
Nutman et al. (2007)	Tonalite	North Atlantic, Greenland	Nuuk region, Itsaq Gneiss Complex	3.85	2	46	Yes
Reimink et al. (2020) [f]	Tonalite, trondhjemite, granodiorite gneiss	Slave, Canada	Acasta Gneiss Complex	4.00-2.94	7 [f]	167 [f]	Yes

Shan et al. (2015)	Tonalite, trondhjemite gneiss	North China	Jiaobei Province	2.50	4	85	Yes
Turkina et al. (2012)	Tonalitic gneiss	Siberian, Russia	Irkut Terrane	2.68	1	6	Yes
Vetrin et al. (2016)	(Rhyo)dacite gneiss	Fennoscandia, Russia	Kola superdeep well	2.84	2	15	No
Vezinet et al. (2018)	Trondhjemite gneiss	North Atlantic, Canada	Saglek Block, Uivak Gneiss	3.86	1	23	Yes
Whitehouse and Kamber (2002a, 2002b)	Tonalite, granodiorite gneiss	North Atlantic, Greenland	Nuuk region, Itsaq Gneiss Complex	3.83	3	57	Partly
Zong et al. (2013)	Trondhjemite gneiss	Tarim, China	Dunhuang area	2.73-2.68	3	57	Yes
Detrital zircon							
Bell et al. (2014)	N/A	Yilgarn, Australia	Jack Hills	4.00-3.35	3	49	N/A
Bell and Harrison (2013)	N/A			4.25-3.82	10	73	N/A
Cavosie et al. (2006)	N/A			4.40-3.65	5	79	N/A
Turner et al. (2020)	N/A			4.20-3.02	1	32	N/A

[a]Preferred crystallization age (or range of ages) for igneous zircon as interpreted in the corresponding reference; [b]Number of igneous or sedimentary samples from which the data were extracted; [c]Total number of individual zircon analyses (before filtering); [d]Availability of whole-rock (WR) compositional data – "Partly" indicates an incomplete dataset (e.g. only some major, or some trace elements); [e]Liu et al. (2013) only report average compositions for igneous zircon in 6 samples, there are therefore only 6 entries for this reference in the database. Those are however calculated from 148 individual zircon analyses; [f]Zircon data compiled from Reimink et al. (2020) specifically exclude 3 samples of the Idiwhaa gneiss unit that are not typical Archean TTGs – this unit has been interpreted as a possible former impact melt (Johnson et al., 2018).

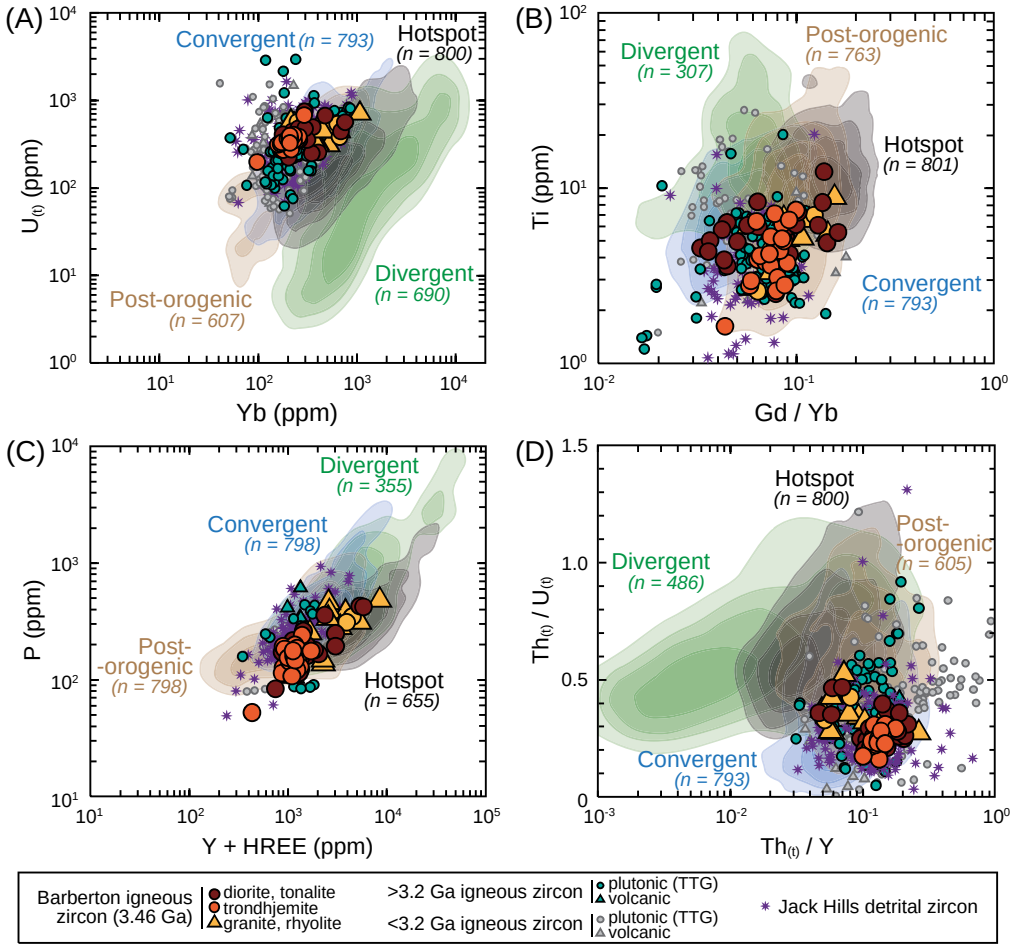

Figure S1: Zircon trace element compositions plotted in $U_{(t)}$ vs. Yb (A) and Ti vs. Gd/Yb (B) from Grimes et al. (2015); P vs. Y + HREE (Gd to Lu) (C) from Belou-sova et al. (2002); and $Th_{(t)}/U_{(t)}$ vs. $Th_{(t)}/Y$. The plots show the similarity between all early Earth zircons and their clustered signature relative to Phanerozoic zircon (fields for various geo-dynamic settings as in main text Figure 4). The sub-script (t) denotes that U and Th contents were corrected from radioactive decay, except for Phanerozoic zircon for which this correction is negligible.

3. Proxies used to filter zircon trace element data for the effects of alteration

Early Earth zircons are prone to radiation damage, as they may show sufficient accumulated alpha-dose for amorphization even at moderate actinide contents (<500 ppm U at >3 Ga; Meldrum et al., 1998). Because radiation-damaged zircon is porous (Geisler et al., 2003a,b) and fractured (Chakoumakos et al., 1987), it is sensitive to fluid-induced chemical modification, resulting in enrichment in LREE, Ca and Fe or replacement by secondary alteration products (Corfu et al., 2003; Geisler et al., 2003a,b; Giéré, 1996; Hoskin, 2005; Kitajima et al., 2012); as well as non-radiogenic Pb uptake and U-Pb discordance (Mezger and Krogstad, 1997; Geisler et al., 2001).

Disturbed zircon compositions can be generally avoided by targeting pristine zircon domains identified by conventional imaging (e.g. Bell et al., 2016; Corfu et al., 2003; Vavra et al., 1999; Zeh et al., 2014). However, even such regions can be affected by post-magmatic disturbance, owing to the presence of altered domains or secondary hydrothermal phases under the imaged surface, or along preferential fluid pathways such as micro-cracks (Bell et al., 2015; Harrison and Schmitt, 2007) and even igneous growth zones (Corfu et al., 2003; Vavra et al., 1999). For this reason, several chemical alteration proxies were proposed in the literature to identify altered zircon:

(1) The **Light Rare Earth Element Index (LREE-I)** of Bell et al. (2016), i.e. the (Dy/Nd)+(Dy/Sm) ratio. The original threshold of Bell et al. (2016) to identify pristine zircon (LREE-I >30) was relaxed here to a **minimum value of 20** to consider uncertainties on the concentrations (not systematically reported in the original publications).

(2) The La concentrations, which show the largest extent of modification during post-magmatic alteration among the REE (Hoskin, 2005). Therefore, slightly altered zircons may have LREE-I >30 but significantly increased La contents. Zeh et al. (2014) considered that pristine zircon was characterized by **La contents normalized to the concentration in C1 chondrite (La_N)** <1, relaxed here to **<2** to consider the (often very large) uncertainties on La concentrations.

(3) The **Ca and Fe concentrations** that should be **below the limit of detection** (l.o.d., generally in the order of ~100 ppm for ICP-MS analyses) in pristine zircon. If l.o.d. was not reported, we used a **maximum Ca and Fe content of 150 ppm**. For Ca, this is based on the threshold of Kitajima et al. (2012) (120 ppm Ca, relaxed here to consider uncertainties). For Fe, this is based on the correlation between LREE-I and Fe of Bell et al. (2016).

(4) Whenever U-Pb isotopic data are available, we considered as reflecting pristine zircon a **degree of discordance <5%** and **fraction of non-radiogenic Pb <1%** (from Zeh et al., 2014), as Pb loss and the presence of common Pb occur preferentially in metamict / altered zircon.

Between 3 and 6 of these alteration proxies were available depending on the data source. Only the zircon analyses positively meeting all criteria were considered as pristine. The disparity in the availability of proxies does not skew the results because the most frequent elimination criteria are LREE-I and La_N (80% of the discarded analyses have LREE-I >20 and 97% have La_N >2), which are both available in all datasets. Figure S2 shows contents in key trace elements plotted against LREE-I. The negative correlation between La, Ti and LREE-I (Fig. S2) possibly reflects the common hydrothermal alteration of zircon to zirconolite ($(Ca,LREE)ZrTi_2O_7$; Giéré, 1996). All other elements (Hf, U, REE, Y) do not seem to be significantly affected by post-magmatic disturbance, with the exception of a few analyses showing higher REE + Y and U (Fig. S2).

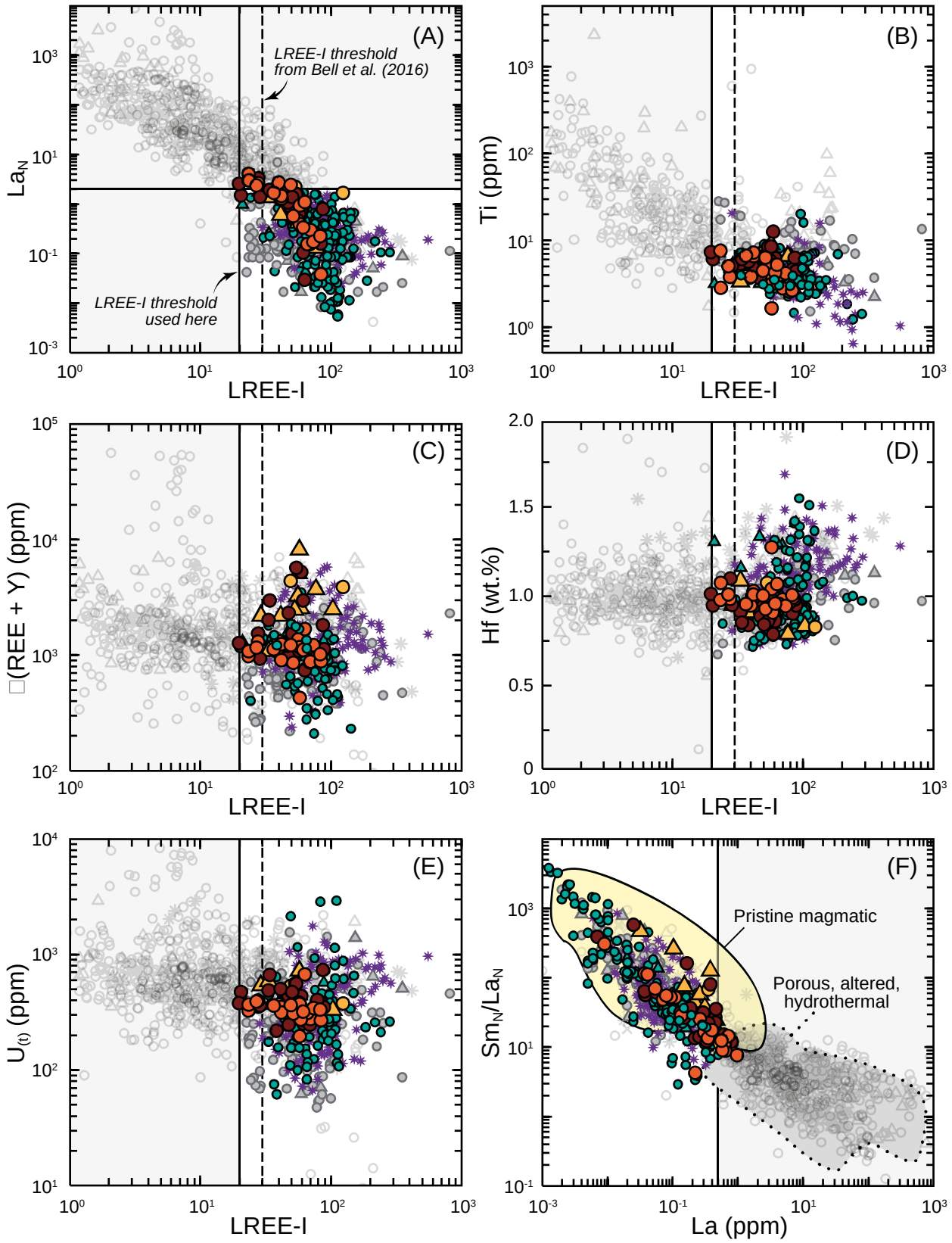

Figure S2: Trace element diagrams showing the compositional differences in the early Earth zircon database between "pristine" data (symbols as in Fig. S1) and analyses affected by post-magmatic disturbance (empty gray symbols). (A–E) Key element concentrations and ratios plotted against the LREE-I index of Bell et al. (2016); and (F) Sm_N/La_N vs. La plot of Hoskin (2005) with compositional fields of pristine and altered zircon from Hoskin (2005) and Grimes et al. (2009). In all plots, the black lines correspond to the filtering thresholds used here and the shaded domains illustrate the compositional ranges excluded thereby. The dashed line corresponds to the lowermost LREE-I limit (30) for pristine zircon of Bell et al. (2016).

4. Details about the zircon/melt partitioning model

This model aims at retrieving the trace element content of the zircon-forming melts from that of zircon itself, using appropriate zircon/melt partition coefficients.

We have excluded the rare earth elements from La to Eu from the modelling for the following two reasons. First, zircon/melt partition coefficients for La, Pr, Nd and Sm vary by 2 to 3 orders of magnitude (see compilation in Claiborne et al., 2018) and the concentrations of these elements in zircon are anyway determined with large uncertainties. Second, the multiple valence states of Ce and Eu make the accurate determination of zircon/melt partition coefficients for these elements impossible without robust constraints on oxygen fugacity upon crystallization (Burnham and Berry, 2012; Smythe and Brenan, 2016; Trail et al., 2012).

Due to possible out-of-equilibrium processes in zircon/melt partitioning experiments, natural partitioning data (e.g. zircon / glass pairs in volcanic rocks) should be preferred (see discussions in Luo and Ayers, 2009; Padilla and Gualda, 2016 and Claiborne et al., 2018). Claiborne et al. (2018) used a newly obtained set of coexisting zircon and glass data in natural volcanic rocks to parametrize two zircon/melt partitioning models based on (1) zircon Ti content or (2) saturation temperature (obtained from the Zr content of the coexisting glass and zircon saturation models). Although for a given element, partition coefficients are generally best correlated with saturation temperature, we used the model based on zircon Ti concentrations. The composition of the coexisting melt is indeed the parameter to constrain here, whereas we measured zircon Ti contents along with other trace elements. The results of the zircon trace element inversion model are shown in Figure 2B of the main paper, and in Figure S3A as well.

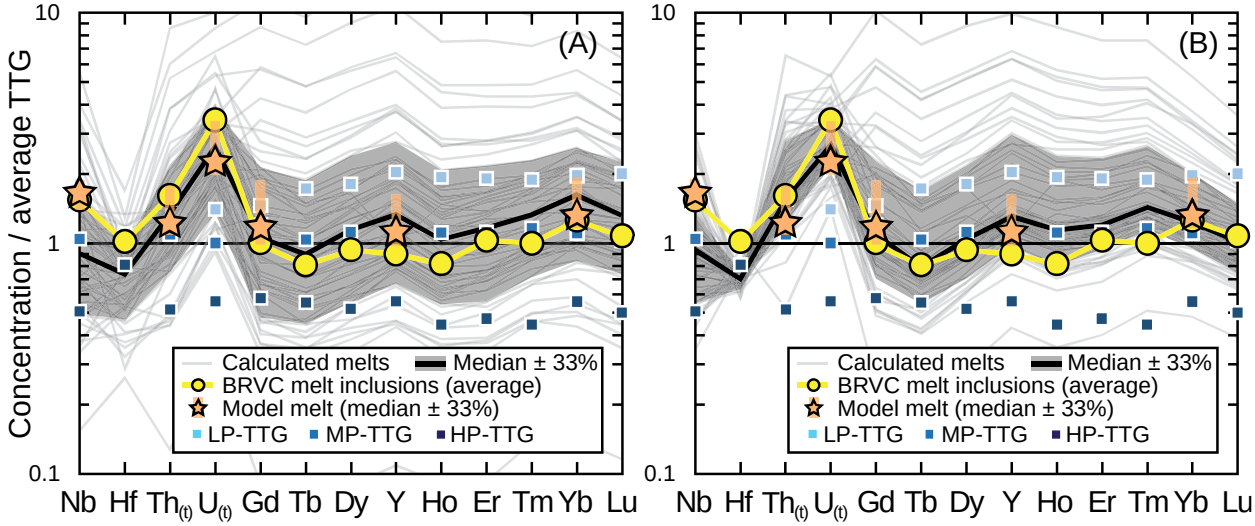

Figure S3: Comparison between trace element concentrations of zircon-forming melts (normalized to average TTG from Moyen, 2011) obtained from inversion of zircon compositions using (A) the partition coefficient parametrization against zircon Ti content of Claiborne et al. (2018) (as in main text Figure 2B) and (B) the median value of partition coefficients compiled in Table S3. The subscript (t) denotes that U and Th contents were corrected from radioactive decay since 3.46 Ga ago.

One potential drawback of this method is that the partition coefficients strongly depend on the parametrization and, in turn, on the calibration dataset – which may or may not be representative of the system to model. In addition, analytical and calibration uncertainties are not propagated in the model of Claiborne et al. (2018) and thus cannot be precisely addressed. To mitigate these sources of uncertainty on the model results, we compared them with a zircon trace element

inversion model based on the median partition coefficient obtained from a compilation (Table S3) of natural zircon/glass data for temperatures and liquid compositions relevant here (i.e. ≤800°C, calc-alkaline systems with granitic melt compositions). The results are shown in Figure S3B.

Table S3: Compiled zircon/melt partition coefficients obtained by measurements of zircon / glass or zircon / melt inclusion pairs in natural volcanic rocks in systems compositionally relevant to this study.

Reference[a]	Nb	Hf	Th	U	Gd	Tb	Dy	Y	Ho	Er	Tm	Yb	Lu
Mahood and Hildreth (1983) [A]	n.d.	3742	91.2	383	n.d.	37	108	n.d.	n.d.	n.d.	n.d.	564	648
Mahood and Hildreth (1983) [B]	n.d.	2645	62.4	298	n.d.	37	95	n.d.	n.d.	n.d.	n.d.	490	635
Fujimaki (1986)	n.d.	971	n.d.	n.d.	6.01	n.d.	44.9	n.d.	n.d.	107	n.d.	516	689
Hinton and Upton (1991)	n.d.	n.d.	n.d.	n.d.	5.01	10.9	23.7	n.d.	48.6	94	171	293	472
Bea et al. (1994)	n.d.	n.d.	22.1	354	9.21	24.8	38.8	71.4	74.5	165	282	278	923
Sano et al. (2002)	n.d.	n.d.	n.d.	n.d.	8	20.7	45.9	n.d.	80	136	197	277	325
Thomas et al. (2002)	n.d.	n.d.	n.d.	n.d.	n.d.	n.d.	22.45	50.2	n.d.	52.72	n.d.	40.63	n.d.
Bachmann et al. (2005)	n.d.	3580	10.6	48.6	19.8	n.d.	106	181	n.d.	274	n.d.	465	n.d.
Colombini et al. (2011) [HRL21]	1.4	3850	50	148	13	34	68	121	134	219	293	359	475
Colombini et al. (2011) [HRL27]	0.18	997	4.5	16	6.2	14	26	46	50	81	122	125	172
Colombini et al. (2011) [KPST01]	0.34	1829	8.1	29	5.8	14	24	42	45	77	105	112	131
Padilla and Gualda (2016)	0.267	2317	7.33	22	11	29	59	80	80	122	128	166	207
Claiborne et al. (2018) [SHL21Z]	0.61	6185	12.69	68.9	25.6	48.41	94.6	166.8	180.5	312.3	447.7	534	752.5
Claiborne et al. (2018) [SHL26Z]	0.32	6424	5.84	90.1	6.83	n.d.	43.2	76.7	n.d.	179.9	n.d.	374.2	488.2
Claiborne et al. (2018) [SHL34Z]	0.67	4494	10.58	98.6	8.68	22.2	49.4	117.5	111.1	189.2	283.5	353	484.9
Median	**0.34**	**3580**	**11**	**90**	**8.3**	**25**	**46**	**78**	**80**	**136**	**197**	**353**	**485**
Median of Kd's obtained using parametrization of Claiborne et al. (2018)	*0.32*	*3403*	*14*	*94*	*9.1*	*23*	*46*	*85*	*97*	*159*	*231*	*286*	*369*

[a]In case several samples were used in a given study, the corresponding sample name is indicated in brackets. "n.d." = not determined.

Clearly, the results obtained using the median partition coefficient obtained from the compilation do not significantly differ from those obtained using the parametrization of Claiborne et al. (2018) (Fig. S3). The main compositional features of the melt remain the same, i.e. a strong enrichment in $Th_{(t)}$ and $U_{(t)}$ and slightly positive slopes for REE spectra from Gd to Lu compared to average TTG (Fig. S3). Importantly, the two datasets (compiled partition coefficients vs. calculated partition coefficients using the model of Claiborne et al., 2018) yield median values that are comparable (Table S3), differing by only 0 to 27% relative, depending on the element. This is remarkable, considering that the database we used in the compilation (15 samples) is largely independent from the calibration dataset of Claiborne et al. (2018) (13 samples), as only 3 samples are common to the two. These observations suggest that the results of our zircon trace element inversion and calculation of equilibrium melts are robust.

5. Methods for thermodynamic modelling of tonalite crystallization

This model considers a batch of magma isolated at some point of its evolution and cooling down at constant pressure. As it crystallizes, the residual melt progressively becomes more felsic until its Zr concentration (hereafter $[Zr]_{melt}$) reaches the saturation value, and zircon starts precipitating. Thus, the calculation uses zircon saturation equations as a proxy for zircon activity – when the liquid is saturated the activity equals one and zircon is a stable phase.

The actual procedure is similar to the setup of e.g. Kelsey et al. (2008) and Schiller and Finger (2019). A phase equilibrium model is first calculated, and the phase proportions as well as melt composition are extracted over the relevant (near-liquidus to sub-solidus) temperature range, as several individual steps. For each temperature step, trace elements are partitioned between the liquid and the solids, allowing to derive $[Zr]_{melt}$ that is compared to Zr solubility at the corresponding temperature and melt chemical composition. If $[Zr]_{melt}$ is lower than melt solubility, the melt is undersaturated and nothing more happens. However, if $[Zr]_{melt}$ exceeds saturation, the excess Zr is used to form zircon, and the trace elements are once more partitioned between liquid and solid – taking zircon into account. Finally, the activities of SiO_2 and TiO_2 are calculated from the thermodynamic properties of the system and used to derive Ti concentration in zircon (Ferry and Watson, 2007).

The starting composition used for modelling is that of the tonalitic "parental liquid" (PL) of the ca. 3.46 Ga Barberton plutonic-volcanic suite, determined by Laurent et al. (2020). Both major and available trace elements (initially modelled by Laurent et al., 2020, i.e. Rb, Sr, Y, Zr, Nb, La, Ce, Sm, Eu, Gd, Yb, Ta, Th, U) were considered. The model was run in the temperature interval 1100–600°C, i.e. from deemed supra-liquidus to sub-solidus conditions, as 150 discrete temperature steps (~3.3 °C each), with 10 extra steps at the solidus to improve the resolution in this region of rapid (eutectic) crystallization. The pressure was set to 3 kbar, considered to be the pressure of emplacement of the Barberton plutons (Anhaeusser, 2010) and in agreement with the composition of the BRVC melt inclusions (Laurent et al., 2020). The initial H_2O content was set to 5 wt.% (corresponding to slightly under-saturated conditions by comparison with relevant experimental melts; Marxer and Ulmer, 2019; Nandedkar et al., 2014; Ulmer, 2017), in agreement with the presence in natural rocks of both hornblende, requiring >4 wt.% H_2O, and relatively sodic plagioclase (An_{20-50}), preventing too high H_2O contents (Laurent et al., 2020). Accordingly, test runs at different H_2O contents, both lower (0.5, 1.0 and 2.0 wt.%) and higher (10 and 20 wt.%), did not satisfactorily reproduce the phase proportions and compositions of natural samples.

5.1. Phase equilibrium modelling

This step is performed using PERPLE_X (Connolly, 2009; Connolly and Petrini, 2002) and the a-X models of (Holland et al., 2018), the latter allowing to calculate the partitioning of TiO_2 and O_2 (or Fe_2O_3) between melts and solids. This turns out to be critical in stabilizing amphibole over clinopyroxene. The system used is NCKFMASHTO (Na-Ca-K-Fe-Mg-Al-Si-H-Ti-O).

In the following, we list for each phase the thermodynamic models used identified by their PERPLE_X name (in v. 6.9.0):

- **Silicate melt:** Melt(HGP) (Holland et al., 2018);
- **Feldspar:** feldspar (Holland and Powell, 2003), split after calculation into plagioclase (0 wt.% K_2O) and K-feldspar (16.9 wt.% K_2O) based on the K_2O content of the mix;
- **Spinel, Cr-spinel and magnetite:** Sp(HGP) (Holland et al., 2018);

- **Garnet:** Gt(HGP) (Holland et al., 2018);
- **Orthopyroxene:** Opx(HGP) (Holland et al., 2018);
- **Cordierite:** Crd(HGP) (Holland et al., 2018 – re-parametrized from White et al., 2014);
- **Biotite:** Bi(HGP) (Holland et al., 2018 – re-parametrized from White et al., 2014);
- **Muscovite:** Mica(W) (White et al., 2014);
- **Epidote:** Ep(HP11) (Holland and Powell, 2011);
- **Hornblende:** cAmph(G) (Green et al., 2016);
- **Ilmenite:** Ilm(WPH) (White et al., 2000).

The predicted phase relations are reasonable, but consistently suffer from two main issues (i) clinopyroxene is systematically predicted as a subsolidus phase replacing hornblende, a fairly unlikely situation that is certainly not observed in intermediate calc-alkaline rocks; (ii) the liquidus temperature is too high (by perhaps 100 or 150 °C), with plagioclase being over-stable at high temperatures. In the context of the current modelling, none is critical, as neither affect the region of interest, the ~150 °C interval above the solidus in which zircon crystallizes.

System properties are extracted in tabular form, and include the proportion and composition of all phases, as well as other thermodynamic properties (chemical potential). The rest of the calculation is performed in a home-made R script available as Supplementary Item.

5.2. Trace element partitioning

Trace element partitioning is calculated using batch equilibration, $C_L = C_0 / (D + F(1-D))$ (Janoušek et al., 2016), where C_L is the composition of the liquid, C_0 the composition of the whole system, F the melt fraction and D, the bulk distribution coefficient, is $D = \sum_i X_i Kd_i$ where Xi is the proportion of mineral i in the solid, and Kd_i its partition coefficient. Two sets of partition coefficients were used: "constant" Kds as compiled in Laurent et al. (2013) for relevant minerals; and "variable" Kd which consider variation of amphibole/melt Kd's, parametrized from the experimental results of Nandedkar et al. (2016) using a temperature-dependent law of the form $log(Kd) = 10^4 a / T(K) + b$ (see Table S4 for a and b parameters). This procedure was used mainly to test to which extent the strongly varying amphibole/melt Kd for Zr in the temperature interval of interest (from ~0.36 at 950°C up to ~2.4 at 780°C; Nandedkar et al., 2016) influences the zircon saturation temperature. Only amphibole/melt partition coefficients were parametrized, since other minerals have little influence on D due to low partition coefficients and/or modal proportions.

Table S4: Fit parameters and correlation coefficient (R^2) for the calculation of Kd of some trace elements in amphibole, based on the experimental results of Nandedkar et al. (2016).

	Zr	**Gd**	**Yb**	**Th**	**U**
a	**0.5018**	**0.4562**	**0.4683**	**0.8386**	**0.9578**
b	**-4.4388**	**-3.3665**	**-3.4920**	**-8.3997**	**-9.4929**
R^2	0.95	0.93	0.94	0.88	0.87

5.3. Zircon saturation

The possible Zr concentration of PL determined by stochastic modelling is 111 ± 88 ppm and shows a uniform distribution within this range (Laurent et al., 2020). However, preliminary tests showed that too Zr-poor systems (<50 ppm) failed to saturate any zircon, in contradiction with observations of natural samples. We therefore considered a starting compositional range of 50 to 200 ppm to determine the possible range of zircon saturation conditions in the model and, in

addition to the potential Kd variations (see section 5.2), bind the model envelope in Figure 4. The calculated $[Zr]_{melt}$ is compared to the saturation value of the melt for the appropriate temperature and composition, derived either from Watson and Harrison (1983) or Boehnke et al. (2013):

$$\ln\left(\frac{[Zr]_{Zrn}}{[Zr]_{melt}}\right) = \left(-3.80 - (0.85\,(M-1))\right) + \frac{12900}{T} \qquad \text{[WH83]}$$

$$\ln\left(\frac{[Zr]_{Zrn}}{[Zr]_{melt}}\right) = \left(-1.48 - (1.16\,(M-1))\right) + \frac{10108}{T} \qquad \text{[B13]}$$

where T is temperature in K, $[Zr]_{Zrn}$ = 497'644 ppm (the stoichiometric Zr content in an ideal zircon) and M is a chemical parameter of the melt based on normalized cation fractions:

$$M = \frac{Na + K + 2Ca}{Al \times Si}$$

The equations are calibrated for $0.9 < M < 1.7$, roughly for $SiO_2 > 60$ %, i.e. well within the range of modelled melt compositions. The B13 equation predicts higher Zr solubilities at near-solidus temperatures, and in Zr-poor systems, this considerably delays or even fully inhibits zircon formation, which contradicts the systematic presence of zircon in natural samples (see discussion in Marxer and Ulmer, 2019). Thus, we also considered the WH83 equation, even though it has notionally been superseded by B13, and regard the range of possible resulting zircon saturation temperatures as an estimate of the uncertainties of the solubility models in the near-solidus region.

If zircon is stable, we calculate its amount by mass balance, assuming that all the Zr in excess of the saturation value of the melt forms stoichiometric zircon. Typical zircon proportions do not exceed 0.01 wt.%. Zr contents in the solids are revised to consider equilibration with the "new" liquid after zircon saturation, and from the definition of partition coefficients ($Kd = C_S / C_L$), the trace element concentration of all phases can be derived.

5.4. Ti incorporation in zircon

Ferry and Watson (2007) established an equation for Ti solubility in zircon that is commonly used as a thermometer:

$$log(Ti_{ppm}) = 5.711(\pm 0.072) - \frac{4800(\pm 86)}{T_K} - log(a_{SiO_2}) + log(a_{TiO_2})$$

This is dependent on the activities of TiO_2 (a_{TiO2}) and SiO_2 (a_{SiO2}) that are not directly output by PERPLE_X. However, they depend on the chemical potential of these elements and the Gibbs free energy of pure phases $\ln a_{TiO_2} = -(G_{ru} - \mu_{TiO_2}) / RT$ and $\ln a_{SiO_2} = -(G_{qz} - \mu_{SiO_2}) / RT$ where G_{ru} and G_{qz} are the Gibbs free energies of rutile and quartz, respectively, and μ the chemical potentials. The latter are output by PERPLE_X and Gibbs free energies are calculated from the thermodynamic database using an ancillary R script adapted from a Matlab code by Jesse Walters (U. Maine, pers. comm., April 2020).

The above permits to calculate directly the Ti concentrations in zircon ($[Ti]_{zircon}$ in Fig. 4) for each temperature interval. This method has the benefit to not rely on unconstrained assumptions on SiO_2 and TiO_2 activities, in contrary to the common approach of using the measured Ti content of zircon as a thermometer. Schiller and Finger (2019) indeed showed that a_{TiO2} may vary between ~0.4 and ~0.8 in near-solidus (granitic) liquids, so that arbitrarily choosing a value in this range propagates significant uncertainties on temperature (at least ± 50°C).

References cited

Anhaeusser, C.R., 2010. Magmatic and structural characteristics of the ca. 3440 Ma Theespruit pluton, Barberton Mountain Land, South Africa. American Journal of Science 310(9), 1136-1167.

Bachmann, O., Dungan, M.A., Bussy, F., 2005. Insights into shallow magmatic processes in large silicic magma bodies: the trace element record in the Fish Canyon magma body, Colorado. Contrib. Mineral. Petrol. 149 (3), 338-349.

Bea, F., Pereira, M.D., Stroh, A., 1994. Mineral/leucosome trace-element partitioning in a peraluminous migmatite (a laser ablation-ICP-MS study). Chem. Geol. 117 (1-4), 291-312.

Bell, E.A., Boehnke, P., Harrison, T.M., 2016. Recovering the primary geochem-istry of Jack Hills zircons through quantitative estimates of chemical alteration. Geochim. Cosmochim. Acta191 (C), 187–202.

Bell, E.A., Boehnke, P., Hopkins-Wielicki, M.D., Harrison, T.M., 2015. Distinguishing primary and secondary inclusion assemblages in Jack Hills zircons. Lithos 234, 15–26.

Bell, E.A., Harrison, T.M., Kohl, I.E., Young, E.D., 2014. Eoarchean crustal evolution of the Jack Hills zircon source and loss of Hadean crust. Geochim. Cosmochim. Acta 146, 27–42.

Bell, E.A. and Harrison, T.M., 2013. Post-Hadean transitions in Jack Hills zircon provenance: a signal of the Late Heavy Bombardment? Earth Planet. Sci. Lett. 364, 1-11.

Belousova, E.A., Griffin, W.L., O'Reilly, S.Y., Fisher, N.I., 2002. Igneous zircon: trace element composition as an indicator of source rock type. Contrib. Mineral. Petrol. 143, 602–622.

Boehnke, P., Watson, E.B., Trail, D., Harrison, T.M., Schmitt, A.K., 2013. Zircon saturation re-revisited. Chem. Geol. 351, 324-334.

Bouvier, A.S., et al., 2012. Li isotopes and trace elements as a petrogenetic tracer in zircon: insights from Archean TTGs and sanukitoids. Contrib. Mineral. Petrol. 163 (5), 745-768.

Burnham, A.D., and Berry, A.J., 2012. An experimental study of trace element partitioning be-tween zircon and melt as a function of oxygen fugacity. Geochim. Cosmochim. Acta 95, 196-212.

Cavosie, A.J., Valley, J.W., Wilde, S.A., E.I.M.F., 2006. Correlated microanalysis of zircon: trace element, d18O, and U–Th–Pb isotopic constraints on the igneous origin of complex >3900 Ma detrital grains. Geochimica et Cosmochimica Acta 70, 5601-5616.

Chakoumakos, B.C., Murakami, T., Lumpkin, G.R., Ewing, R.C., 1987. Alpha-decay-induced fracturing in zircon: the transition from the crystalline to the metamict state. Science 236, 1556-1559.

Claiborne, L.L., et al., 2018. Zircon as Magma Monitor: Robust, Temperature-Dependent Partition Coefficients from Glass and Zircon Surface and Rim Measurements from Natural Systems. *In* Moser, D.E., Corfu, F., Darline, J.R., Reddy, S.M., and Tait, K. (eds.): Microstructural Geochronology: Planetary Records Down to Atom Scale. Geophysical Monograph 232, John Wiley & Sons, p. 3-34.

Colombini, L.L., Miller, C.F., Gualda, G.A.R., Wooden, J.L., Miller, J.S., 2011. Sphene and zircon in the Highland Range volcanic sequence (Miocene, southern Nevada, USA): elemental partitioning, phase relations, and influence on evolution of silicic magma. Mineral. Petrol. 102(1-4), 29-50.

Connolly, J.A.D., 2009. The geodynamic equation of state: what and how. Geochem. Geophys. Geosyst. 10, Q10014.

Connolly, J.A.D., Petrini, K., 2002. An automated strategy for calculation of phase diagram sections and retrieval of rock properties as a function of physical conditions. J. Metamorph. Geol. 20, 697-708.

Corfu, F., Hanchar, J.M., Hoskin, P.W.O., Kinny, P., 2003. Atlas of zircon textures. *In* Hanchar, J.M., Hoskin, P.W.O. (eds.): Zircon. Reviews in Mineralogy 53, pp. 468-500.

Ferry, J., Watson, E., 2007. New thermodynamic models and revised calibrations for the Ti-in-zircon and Zr-in-rutile thermometers. Contrib. Mineral. Petrol. 154, 429-437.

Fujimaki, H., 1986. Partition coefficients of Hf, Zr, and REE between zircon, apatite, and liquid. Contributions to Mineralogy and Petrology 94, 42-45.

Geisler, T., Pidgeon, R.T., von Bronswijk, W.V., Pleysier, R., 2001. Kinetics of thermal recovery and recrystallization of partially metamict zircon, a Raman spectroscopic study. Eur. J. Mineral. 13, 1163-1176.

Geisler, T., Pidgeon, R.T., Kurtz, R., Bronswijk, W.V., Schleicher, H., 2003a. Experimental hydrothermal alteration of partially metamict zircon. Am. Mineral. 88, 1496-1513.

Geisler, T., Rashwan, A.A., Rahn, M.K.W., Poller, U., Zwingmann, H., Pidgeon, R.T., Schleicher, H., Tomaschek, F., 2003b. Low-temperature hydrothermal alteration of natural metamict zircons from the Eastern Desert, Egypt. Mineral. Mag. 67, 485-508.

Gieré, R., 1996. Formation of rare earth minerals in hydrothermal systems. *In* Jones, A.P., Wall, F., Williams, C.T. (eds.): Rare Earth Minerals: Chemistry, origin and ore deposits, Chapman and Hall, London, UK, pp. 105-150.

Green, E., White, R., Diener, J., Powell, R., Holland, T., Palin, R., 2016. Activity–composition relations for the calculation of partial melting equilibria in metabasic rocks. J. Metamorph. Geol. 34, 845-869.

Grimes, C.B., et al., 2009. On the occurrence, trace element geochemistry, and crystallization history of zircon from in situ ocean lithosphere: Contrib. Mineral. Petrol. 158, 757–783.

Harrison, T.M., and Schmitt, A.K., 2007. High sensitivity mapping of Ti distributions in Hadean zircons. Earth Planet. Sci. Lett. 261, 9-19.

Hellstrom, J.C., et al., 2008. Iolite: Software for spatially resolved LA-(quad and MC) ICP-MS analysis. *In* Sylvester, P. (ed.): Laser ablation ICP-MS in the Earth sciences: Current practices and outstanding issues. Mineralogical Association of Canada, Vancouver, pp. 343-348.

Hinton, R.W., and Upton, B.G.J., 1991. The chemistry of zircon: variations within and between large crystals from syenite and alkali basalt xenoliths. Geochim. Cosmochim. Acta 55, 3287-3302.

Holland, T., Powell, R., 2003. Activity–composition relations for phases in petrological calculations: an asymmetric multicomponent formulation. Contrib. Mineral. Petrol. 145, 492-501.

Holland, T.J., Green, E.C., Powell, R., 2018. Melting of peridotites through to granites: a simple thermodynamic model in the system KNCFMASHTOCr. J. Petrol. 59, 881-900.

Holland, T.J.B., Powell, R., 2011. An improved and extended internally consistent thermodynamic dataset for phases of petrological interest, involving a new equation of state for solids. J. Metamorph. Geol. 29, 333-383.

Hoskin, P.W.O., 2005. Trace-element composition of hydrothermal zircon and the alteration of Hadean zircon from the Jack Hills, Australia. Geochim. Cosmochim. Acta 69, 637-648.

Janoušek, V., Moyen, J.F., Martin, H., Erban, V., Farrow, C.M., 2016. Geochemical Modelling of Igneous Processes—Principles and Recipes in the R Language. Springer Verlag, Berlin.

Jochum, K.P., et al., 2011. Determination of Reference Values for NIST SRM 610-617 Glasses Following ISO Guidelines. Geostandards and Geoanalytical Research 35(4), 397-429.

Johnson, T.E., et al., 2018. An impact melt origin for Earth's oldest known evolved rocks. Nature Geoscience 11, 795-199.

Kelsey, D.E., Clark, C., Hand, M., 2008. Thermobarometric modelling of zircon and monazite growth in melt–bearing systems: examples using model metapelitic and metapsammitic granulites. J. Metamorph. Geol. 26, 199-212.

Kennedy, A.K., et al., 2014. Eocene zircon reference material for microanalysis of U-Th-Pb isotopes and trace elements. The Canadian Mineralogist 52(3), 409-421.

Kielman, R., Whitehouse, M., Nemchin, A., Kemp, A., 2018. A tonalitic analogue to ancient detrital zircon. Chemical Geology 499, 43–57.

Kitajima, K., Ushikubo, T., Kita, N.T., Maruyama, S., Valley, J.W., 2012. Relative retention of trace element and oxygen isotope ratios in zircon from Archean rhyolite, Panorama Formation, North Pole Dome, Pilbara Craton, Western Australia. Chemical Geology 332–333, 102-115.

Laurent, O., Doucelance, R., Martin, H., Moyen, J.-F., 2013. Differentiation of the late-Archaean sanukitoid series and some implications for crustal growth: Insights from geochemical modelling on the Bulai pluton, Central Limpopo Belt, South Africa. Precambrian Research 227, 186-203.

Laurent, O., et al., 2020. Earth's earliest granitoids are crystal-rich magma reservoirs tapped by silicic eruptions. Nature Geoscience 13, 163-169.

Liu, J., et al., 2013. The growth, reworking and metamorphism of early Precambrian crust in the Jiaobei terrane, the North China Craton: Constraints from U–Th–Pb and Lu–Hf isotopic systematics, and REE concentrations of zircon from Archean granitoid gneisses. Precambrian Research 224, 287-303.

Luo, Y., and Ayers, J.C., 2009. Experimental measurements of zircon/melt trace element partition coefficients. Geochim. Cosmochim. Acta 73(12), 3656-3679.

Mahood, G., and Hildreth, W., 1983. Large partition coefficients for trace elements in high-silica rhyolites. Geochim. Cosmochim. Acta 47(1), 11-30.

Marxer, F., and Ulmer, P., 2019. Crystallization and zircon saturation of calc-alkaline tonalite from the Adamello Batholith at upper crustal conditions: an experimental study. Contributions to Mineralogy and Petrology 174, 84.

Meldrum, A., Boatner, L.A., Weber, W.J., Ewing, R.C., 1998. Radiation damage in zircon and monazite. Geochimica et Cosmochimica Acta 62, 2509-2520.

Mezger, K., and Krogstad, E.J., 1997. Interpretation of discordant U-Pb zircon ages: an evaluation. J. Metamorph. Geol. 15, 127-140.

Moyen, J.-F., 2011. The composite Archaean grey gneisses: Petrological significance, and evidence for a non-unique tectonic setting for Archaean crustal growth: Lithos 123(1–4), 21–36.

Nandedkar, R., Ulmer, P., Müntener, O. (2014). Fractional crystallization of primitive, hydrous arc magmas: an experimental study at 0.7 GPa. Contributions to Mineralogy and Petrology 167, 1015.

Nandedkar, R.H., Hürlimann, N., Ulmer, P., Müntener, O., 2016. Amphibole–melt trace element partitioning of fractionating calc-alkaline magmas in the lower crust: an experimental study. Contrib. Mineral. Petrol. 171, 71.

Nutman, A.P., Bennett, V.C., Friend, C.R.L., Horie, K., Hidaka, H., 2007. ~3,850 Ma tonalites in the Nuuk region, Greenland: geochemistryand their reworking within an Eoarchaean gneiss complex. Contrib. Mineral. Petrol. 154, 385–408.

Padilla, A.J., and Gualda, G.A.R., 2016. Crystal-melt elemental partitioning in silicic magmatic systems: An example from the Peach Spring Tuff high-silica rhyolite, Southwest USA. Chemical Geology 440, 326-344.

Reimink, J.R., Davies, J.H.F.L., Bauer, A.M., Chacko, T., 2020. A comparison between zircons from the Acasta Gneiss Complex and the Jack Hills region. Earth and Planetary Science Letters 531, 115975.

Sano, Y., Terada, K., Fukuoka, T., 2002. High mass resolution ion microprobe analysis ofrare earth elements in silicate glass, apatite and zircon: lack of matrix dependency. Chem. Geol. 184(3-4), 217-230.

Schiller, D., Finger, F., 2019. Application of Ti-in-zircon thermometry to granite studies: problems and possible solutions. Contrib. Mineral. Petrol. 174, 51.

Shan, H., et al., 2015. Zircon U–Pb ages, geochemistry, and Nd–Hf isotopes of the TTG gneisses from the Jiaobei terrane: Implications for Neoarchean crustal evolution in the North China Craton. J. Asian Earth Sci. 98, 61-74.

Sláma, J., et al., 2008. Plešovice zircon - A new natural reference material for U-Pb and Hf isotopic microanalysis. Chemical Geology 249, 1-35.

Smythe, D.J., and Brenan, J.M., 2016. Magmatic oxygen fugacity estimated using zircon-melt partitioning of cerium. Earth and Planetary Science Letters 453, 260-266.

Szymanowski, D., et al., M., 2018. Isotope-dilution anchoring of zircon reference materials for accurate Ti-in-zircon thermometry. Chemical Geology 481, 146-154.

Thomas, J.B., Bodnar, R.J., Shimizu, N., Sinha, A.K., 2002. Determination of zircon/melttrace element partition coefficients from SIMS analysis of melt inclusions in zircon. Geochim. Cosmochim. Acta 66(16), 2887-2901.

Trail, D., Watson, E.B., Tailby, N.D., 2012. Ce and Eu anomalies in zircon as proxies for the oxidation state of magmas. Geochimica et Cosmochimica Acta 97, 70-87.

Turkina, O.M., Berezhnaya, N.G., Lepekhina, E.N., Kapitonov, I.N., 2012. U–Pb (SHRIMP II), Lu–Hf isotope and trace element geochemistry of zircons from high-grade metamorphic rocks of the Irkut terrane, Sharyzhalgay Uplift: Implications for the Neoarchaean evolution of the Siberian Craton. Gondwana Research 21, 801-817.

Turner, S., Wilde, S., Wörner, G., Schaefer, B., Lai, Y.J., 2020. An andesitic source for Jack Hills zircon supports onset of plate tectonics in the Hadean. Nature Communications 11, 1241.

Ulmer, P., Kägi, R., Müntener, O., 2018. Experimentally Derived Intermediate to Silica-rich Arc Magmas by Fractional and Equilibrium Crystallization at 1.0 GPa: an Evaluation of Phase Relationships, Compositions, Liquid Lines of Descent and Oxygen Fugacity. Journal of Petrology 59(1), 11-58.

Vavra, G., Schmid, R., Gebauer, D., 1999. Internal morphology, habit and U–Th–Pbmicroanalysis of amphibolite-to-granulite facies zircons: geochronology of theIvrea Zone (Southern Alps). Contributions to Mineralogy and Petrology 134, 380-404.

Vetrin, V.R., Belousova, E.A., Chupin, V.P., 2016. Trace Element Composition and Lu-Hf Isotope Systematics of Zircon from Plagiogneisses of the Kola Superdeep Well: Contribution of a Paleoarchean Crust in Mesoarchean Metavolcanic Rocks. Geochemistry International 54(1), 92-111.

Vezinet, A., Pearson, D.G., Thomassot, E., Stern, R.A., Sarkar, C., Luo, Y., Fisher, C.M., 2018. Hydrothermally-altered mafic crust as source for early Earth TTG: Pb/Hf/O isotope and trace element evidence in zircon from TTG of the Eoarchean Saglek Block, N. Labrador. Earth and Planetary Science Letters 503, 95-107.

Watson, E.B., Harrison, T.M., 1983. Zircon saturation revisited: temperature and composition effects in a variety of crustal magmas types. Earth Planet. Sci. Lett. 64, 295-304.

White, R., Powell, R., Holland, T., Johnson, T., Green, E., 2014. New mineral activity–composition relations for thermodynamic calculations in metapelitic systems. J. Metamorph. Geol. 32, 261-286.

White, R.W., Powell, R., Holland, T.J.B., Worley, B., 2000. The effect of TiO_2 and Fe_2O_3 on metapelitic assemblages at greenschist and amphibolite facies conditions: mineral equilibria calculations in the system K_2O–FeO–MgO–Al_2O_3–SiO_2–H_2O–TiO_2–Fe_2O_3. J. Metamorph. Geol. 18, 497-511.

Whitehouse, M.J., and Kamber, B.S., 2002. A rare earth element study of complex zircons from early Arcaean Amîtsoq gneisses, Godthåbsfjord, south-west Greenland. Precambrian Research 126, 363-377.

Whitney, D.L., and Evans, B.W., 2010. Abbreviations for names of rock-forming minerals. Am. Mineral. 95, 185–187.

Wiedenbeck, M., et al., 1995. Three natural zircon standards for U-Th-Pb, Lu-Hf, trace element and REE analyses. Geostandards Newsletter 19, 1-23.

Zong, K., Liu, Y., Zhang, Z., He, Z., Hu, Z., Guo, J., Chen, K., 2013. The generation and evolution of Archean continental crust in the Dunhuang block, northeastern Tarim craton, northwestern China. Precambrian Research 235, 251-263.